

# ***E*-selective Semi-hydrogenation of Alkynes Under Mild Conditions by a Diruthenium Hydride Complex**

Cody B. van Beek,<sup>a,#</sup> Lars Killian,<sup>a,#</sup> Martin Lutz,<sup>b</sup> Markus Weingarth,<sup>c</sup> Arun S. Asundi,<sup>d</sup> Ritimukta Sarangi,<sup>d</sup> Robertus. J. M. Klein Gebbink<sup>a</sup> and Daniël L. J. Broere<sup>\*a</sup>

<sup>a</sup> Organic Chemistry and Catalysis, Debye Institute for Nanomaterials Science, Faculty of Science, Utrecht University Universiteitsweg 99, 3584 CG, Utrecht (The Netherlands). E-mail: [d.l.j.broere@uu.nl](mailto:d.l.j.broere@uu.nl)

<sup>b</sup> Structural Biochemistry, Bijvoet Centre for Biomolecular Research, Faculty of Science, Utrecht University Universiteitsweg 99, 3584 CG, Utrecht (The Netherlands)

<sup>c</sup> NMR Spectroscopy, Bijvoet Centre for Biomolecular Research, Department of Chemistry, Faculty of Science, Utrecht University, Padualaan 8, 3584 CH Utrecht, The Netherlands.

<sup>d</sup> Stanford Synchrotron Radiation Lightsource, SLAC National Accelerator Laboratory, Stanford University, 94025, Menlo Park, California (USA)

<sup>#</sup> Both authors contributed equally to this work

## **Abstract**

Reacting the <sup>t</sup>BuPNNP expanded pincer ligand with two equiv of RuHCl(PPh<sub>3</sub>)<sub>3</sub>(CO) at high temperatures produces an insoluble air-stable complex, which was structurally characterized as [Ru<sub>2</sub>(<sup>t</sup>BuPNNP)H(μ-H)Cl(μ-Cl)(CO)<sub>2</sub>] using solid-state NMR, IR and X-ray absorption spectroscopies and follow-up reactivity. A reaction with KO<sup>t</sup>Bu results in deprotonation of a methylene linker to produce a soluble complex featuring a partially dearomatized naphthyridine core. This enables metal-ligand cooperative activation of H<sub>2</sub> analogous to the mononuclear analogue, [Ru(<sup>t</sup>BuPNP\*)H(CO)]. In contrast to the mononuclear system, the bimetallic analogue produces an active catalyst for the *E*-selective semi-hydrogenation of alkynes under mild conditions (ambient temperature and pressure) with good functional group tolerance. Monitoring this reaction using <sup>1</sup>H NMR spectroscopy for the hydrogenation of diphenylacetylene shows the intermediacy of *Z*-stilbene, which is subsequently isomerized to the *E*-isomer. Initial findings into the mode of action of this system are provided, including the spectroscopic characterization of a polyhydride intermediate and the isolation of a deactivated species with a partially hydrogenated naphthyridine backbone.

## **Introduction**

The selective semi-hydrogenation of alkynes to alkenes is an important reaction in organic synthesis.<sup>1</sup> Selective conversion of alkynes to *Z*-alkenes is well established using either heterogeneous Lindlar catalyst (poisoned Pd-based)<sup>2</sup> or homogeneous catalyst systems such as the Wilkinson or Schrock/Osborn catalysts.<sup>3,4</sup> In contrast, *E*-alkenes are commonly prepared from alkynes by a Na/NH<sub>3</sub> based stoichiometric reduction, which suffers from poor functional group tolerance and produces stoichiometric amounts of waste.<sup>5</sup> As such, the atom-economical *E*-selective semi-hydrogenation of alkynes using H<sub>2</sub> is still considered as a challenging reaction for the preparation of *E*-alkenes.<sup>6</sup> In the last decade several homogeneous catalysts have been reported for the *E*-selective semi-hydrogenation of alkynes<sup>7,8</sup> based on platinum group metal systems (Pd,<sup>9</sup> Ir,<sup>10</sup> Ru,<sup>11</sup> heterobimetallic Ag-Ru and Ru-Ir<sup>12</sup>) as well as first row transition metal systems (Mn,<sup>13</sup> Fe,<sup>8a</sup> Co,<sup>8b</sup> Ni<sup>8d,13,14</sup>). However, there are few systems<sup>7a,14,15</sup> that enable the *E*-selective semi-hydrogenation at ambient temperatures and pressures of compounds that contain other functional groups that are susceptible to hydrogenation.

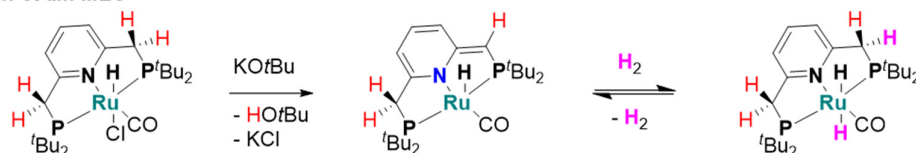
Inspired by natural metalloenzymes, chemists have developed various platforms that mediate making and breaking of chemical bonds through the cooperative interplay between a metal and a bound ancillary ligand.<sup>16</sup> Such metal ligand cooperativity (MLC) has been exploited to catalyze various chemical transformations under milder conditions or with increased selectivity. A prominent platform in this field is Milstein's ruthenium

hydrido carbonyl complex containing a pyridine-based PNX (X = P, N) pincer ligand, which enables cooperative bond activation through reversible dearomatization of the ligand backbone (Scheme 1, top). These systems have found wide application in a variety of (de)hydrogenative transformations of polar bonds,<sup>17</sup> but have not been reported for the selective semi-hydrogenation of alkynes to the best of our knowledge.<sup>18</sup>

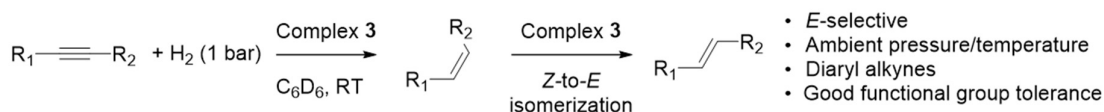
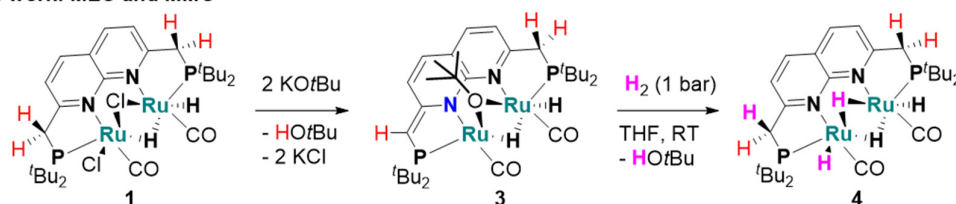
Another avenue in the field of cooperative bond activation and catalysis that is gaining increased attention involves well-defined systems that utilize the cooperative action of multiple metal atoms in close proximity.<sup>19</sup> In such systems metal-metal cooperativity (MMC) enables distinct reactivity or selectivity from mononuclear analogues.<sup>20</sup> Dinucleating ligands containing a 1,8-naphthyridine core are well suited for the preparation of bimetallic complexes, as shown by the wide range of ligand scaffolds that have recently been disclosed.<sup>21</sup> In our group, we have developed PNNP ‘expanded pincer’ ligands that can bind two metal atoms in close proximity to allow for MMC.<sup>22</sup> Moreover, we have demonstrated that reversible dearomatization of the naphthyridine backbone allows for heterolytic bond activation through MLC. Inspired by these findings and the pivotal role of Milstein’s pincer bound ruthenium hydrido carbonyl complexes in hydrogenation catalysis, we set out to synthesize the related bimetallic complex and investigate its reactivity in hydrogenative transformations.

Herein, we describe the synthesis and characterization of several diruthenium(II) hydrido carbonyl complexes supported by a PNNP expanded pincer ligand (Scheme 1). Deprotonation of the methylene linkers in these complexes enables metal-ligand cooperative activation of dihydrogen to give an active catalyst for the *E*-selective semi-hydrogenation of internal alkynes. We show how the diruthenium catalyst enables this transformation with good functional group tolerance under exceptionally mild conditions. Finally, we provide initial insights into the operating mechanism of this transformation, including the spectroscopic observation of a key intermediate and the isolation of a deactivated species with an unusual structure.

**Milstein et al.: MLC**



**This work: MLC and MMC**

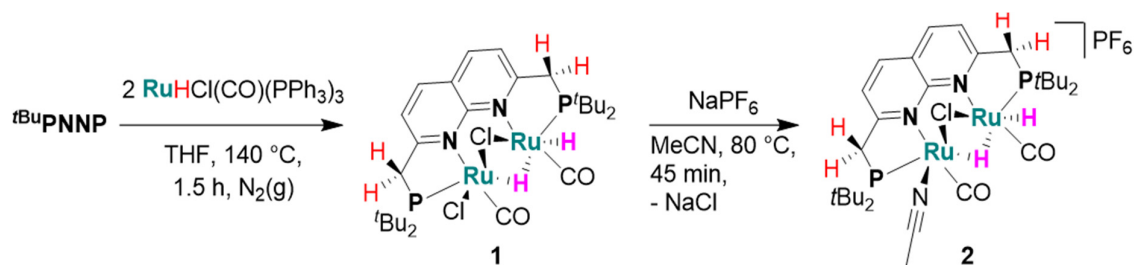


- *E*-selective
- Ambient pressure/temperature
- Diaryl alkynes
- Good functional group tolerance

**Scheme 1:** Comparison between Milstein’s PNP and the PNNP system for cooperative H<sub>2</sub> activation and application for *E*-selective alkyne semi-hydrogenation.

**Synthesis and characterization**

Reacting <sup>t</sup>BuPNNP with two equiv of RuHCl(PPh<sub>3</sub>)<sub>3</sub>(CO) in THF at 140 °C results in the precipitation of [Ru<sub>2</sub>(<sup>t</sup>BuPNNP)H(μ-H)Cl(μ-Cl)(CO)<sub>2</sub>] (**1**) as an air-stable orange powder in 75% yield. Its insolubility in organic solvents prohibited the formation of good-quality crystals and characterization by solution NMR spectroscopy. However, extensive analysis and follow-up reactivity of complex **1** (see below) we propose a structure as depicted in Scheme 2.



**Scheme 2:** The synthesis of complex **1** from  $t\text{BuPNNP}$  and  $\text{RuHCl}(\text{PPh}_3)_3(\text{CO})$ .

Heating a suspension of complex **1** and  $\text{NaPF}_6$  in acetonitrile at  $80\text{ }^\circ\text{C}$  results in halide abstraction to give air-stable  $[\text{Ru}_2(t\text{BuPNNP})\text{H}(\mu\text{-H})\text{MeCN}(\mu\text{-Cl})(\text{CO})_2]\text{PF}_6$  (**2**) as an orange solid in 30% yield (Scheme 2).<sup>23</sup> The ATR-IR spectrum of complex **2** (Fig S18) shows two strong bands at  $\nu = 1972$  and  $1938\text{ cm}^{-1}$  corresponding to two terminal bound CO ligands. Furthermore, a weak band at  $\nu = 2069\text{ cm}^{-1}$  shows the presence of a terminal hydride ligand.<sup>17c</sup> The  $^{31}\text{P}\{^1\text{H}\}$  NMR spectrum of **2** in acetonitrile- $d_3$  at 298 K displays two signals at  $\delta = 109.4$  and  $107.1$  ppm and the characteristic resonance for the  $\text{PF}_6^-$  anion. The  $^1\text{H}$  NMR spectrum of **2** in acetonitrile- $d_3$  at 298 K displays four doublets in the aromatic region, suggesting a lack of symmetry perpendicular to the naphthyridine plane. Additionally, four different doublets of doublets resonances for the four methylene linker protons are observed, showing that the ligand environment is different above and below the naphthyridine plane. Furthermore, two resonances are found at  $\delta = -14.52$  (doublet) and  $-15.80$  ppm (doublet of doublets) corresponding to a terminal and bridging hydride ligand, respectively, based on extensive 2D analysis (see ESI). A singlet at  $\delta = 1.96$  ppm that integrates for 3H is assigned to unbound acetonitrile that is exchanged for an acetonitrile- $d_3$  ligand. Single crystals of **2** suitable for X-ray crystal structure determination were grown from a standing saturated benzene solution at ambient temperature. While being inconclusive about the hydrogen atoms, the overall molecular structure (Figure 1) in the crystal is consistent with the NMR results in solution (see ESI). Two Ru centers are bound within the  $t\text{BuPNNP}$  ligand that have inequivalent coordination environments, which is in agreement with the NMR data. Ru11 has distorted octahedral geometry and shows a bound bridging chloride and a terminal bound acetonitrile and terminal carbonyl ligand, whereas Ru21 with distorted octahedral geometry has a bridging chloride ligand, a terminal carbonyl ligand and hydride ligands. The hydride ligands, one terminal and one bridging, were placed at calculated positions, resulting in a 18 valence electron (VE) count for both metal centers.<sup>24</sup> Although the Ru-Ru distance of  $2.8149(10)\text{ \AA}$  is shorter than the sum of the covalent radii of  $2.92\text{ \AA}$ ,<sup>25</sup> a Ru-Ru bond is unlikely to be present.<sup>26</sup>

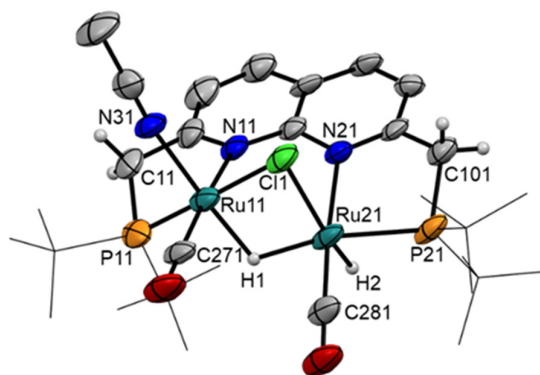


**Figure 1:** Displacement ellipsoid plot (50% probability) of the asymmetric unit of cationic complex **2** with the  $t\text{Bu}$  groups on P depicted as wireframe for clarity. The  $\text{PF}_6^-$  anion, benzene molecules, and most hydrogen atoms are omitted. The hydride ligands are introduced in calculated positions. Ru11-Ru21  $2.8149(10)\text{ \AA}$ , Ru11-P11  $2.277(4)\text{ \AA}$ , Ru11-N11  $2.169(6)\text{ \AA}$ , Ru11-Cl1  $2.482(3)\text{ \AA}$ , Ru11-N31  $2.101(7)\text{ \AA}$ , Ru11-C271  $1.844(9)\text{ \AA}$ , Ru21-P21  $2.275(3)\text{ \AA}$ , Ru21-N21  $2.214(6)\text{ \AA}$ , Ru21-Cl1  $2.528(2)\text{ \AA}$ , Ru21-C281  $1.807(9)\text{ \AA}$ .

The spectroscopic characterization and structural insights of complex **2** allows for a more substantiated proposal for the structure of complex **1** through the comparison of the spectroscopic data. The ATR-IR spectrum of complex **1** (Fig S4) displays two strong terminal CO bands at  $\nu = 1942$  and  $1905\text{ cm}^{-1}$ , which are at similar energies as in **2**. Another similarity with complex **2**, is the presence of a weak absorption at  $\nu = 2021\text{ cm}^{-1}$ , which indicates the presence of a terminal Ru-H bond.<sup>17c</sup> The  $^1\text{H}$  solid-state NMR (ssNMR) spectrum (Fig S1) is dominated by a strong signal at  $\delta = 1.2$  ppm, corresponding to the *-t*Bu substituents. Several aromatic signals up to 9.7 ppm and resonances between 2.8-4.6 ppm are observed. Notably, four distinct resonances in the hydride region are observed at  $\delta = -14.3$  (major),  $-15.1$  (minor),  $-16.8$  (major) and  $-18.8$  (minor) ppm with an integral ratio 1 to 0.1-0.2 between the major and minor set of resonances, respectively. The 1 to 0.1-0.2 ratio of the integrals suggest that two populations are present, which can be assigned to the presence of two different isomers or by different polymorphs of complex **1**.<sup>27</sup> The  $^{31}\text{P}$  ssNMR spectrum (Fig S2) displays two main peaks at  $\delta = 110.6$  and  $106.8$  ppm that are not well resolved, but at comparable chemical shifts as the resonances observed in the solution  $^{31}\text{P}$  NMR spectra of **2**. The  $^{13}\text{C}$  ssNMR spectrum (Figure S3) displays two major resonances in the range of  $\delta = 205$ - $210$  ppm and a minor resonance at  $\delta = 210$  ppm. These features are at similar chemical shifts as the resonances assigned to the carbonyl ligands in the solution spectra of **2** at  $\delta = 206$  and  $201$  ppm (Fig S8). The similar spectroscopic features in the NMR and IR spectra of **1** and **2** suggests that no major structural rearrangements occur upon chloride abstraction from **1**. CHN combustion analysis also is in agreement with the proposed structure of **1**.

To address the question whether different isomers are present in complex **1**, we evaluated the possibility of four isomers. These proposed isomers differ solely in the arrangement of their bridging and terminal chloride and hydride ligands and still all have one terminal carbonyl ligand per ruthenium center in the plane of the naphthyridine ligand (Figure S54). The relative stability of these isomers were computationally assessed by comparison of the relative energies of the DFT optimized gas phase geometries (BP86/def2-TZVP level) of these isomers (Figure S54). This showed that the geometry of complex **1** has the lowest energy. Alternative isomer 2, where the chlorides and hydrides are not both on the same side of the of the naphthyridine plane is  $7.9\text{ kcal mol}^{-1}$  higher in energy. In addition, an isomer that is not consistent with the spectroscopic data above, featuring two bridging hydrides and two terminal chlorides was found to be  $8.8\text{ kcal mol}^{-1}$  higher in energy than complex **1** (see ESI).

In the absence of metrical parameters and to better assess the isomers of **1** we sought to obtain more insights through X-ray absorption near edge structure (XANES) and extended X-ray absorption fine structure (EXAFS) analysis. Ru K-edge X-ray absorption spectra were measured on a solid pellet sample of **1** and are presented in Figure 2. The rising edge energy at a normalized absorbance of 0.5 is  $22112.2\text{ eV}$  for **1** compared to  $22110.8\text{ eV}$  for the reference Ru metal, consistent with an increase in oxidation state of Ru in **1** (Figure Xa). The FEFF model of the EXAFS (Figure 2b, Table S1) supports the DFT-optimized structure (BP86/def2-TZVP, see Figure S53), with 1 Ru-C at  $1.82\text{ \AA}$ , 1 Ru-N at  $2.16\text{ \AA}$ , 1 Ru-P at  $2.28\text{ \AA}$ , 1.5 Ru-Cl at  $2.48\text{ \AA}$ . The EXAFS fit yielded a Ru-Ru distance of  $2.81\text{ \AA}$ . These metric parameters are similar to those found for **2** by single-crystal X-ray structure analysis. Two Ru-C-O paths were required to fit the data well. The necessity to include these paths indicates a linearly bound CO ligand on each Ru atom, which significantly contributes to the Ru EXAFS. The EXAFS measurement provides experimental support for the structure of **1** obtained from DFT. The DFT bond lengths of isomer 2 are very similar to those of compound **1**, and thus the potential presence of isomer 2, as indicated by NMR, cannot be distinguished from a pure sample of compound **1** by this EXAFS measurement. In contrast, the computed Ru-Ru bond length in isomer 1 is  $2.68\text{ \AA}$ , significantly shorter than that measured by EXAFS. Together, the NMR, DFT, and EXAFS results show that the major product obtained when  $^{\text{tBu}}\text{PNNP}$  is reacted with two equivalents of  $\text{RuHCl}(\text{PPh}_3)_3(\text{CO})$  has the structure of complex **1** and the minor product of isomer 2. Given that we do not observe a different isomer in the synthesis of **2** we reason that isomerization is facile upon halide abstraction or other reactivity (see below).

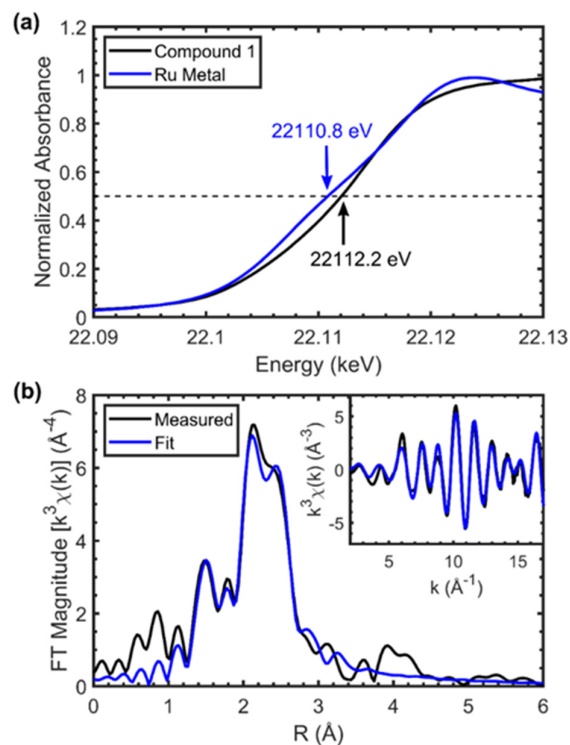
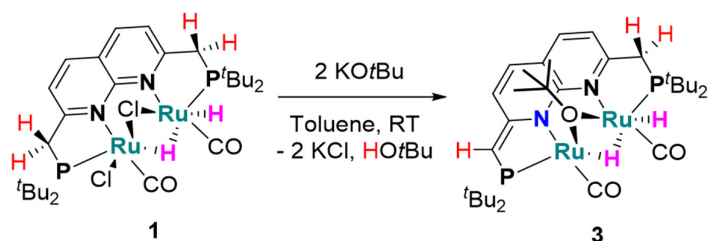


**Figure 2.** (a) Ru K-edge XANES for **1** and a Ru metal reference. (b) Magnitude of the  $k^3$ -weighted EXAFS Fourier Transform and model fit for **1**. Inset: EXAFS and fit in  $k$ -space with  $k^3$  weighting. Spectra were fit in a  $k$ -range of 2-17  $\text{\AA}^{-1}$  and an  $R$ -range of 1-3  $\text{\AA}$ . Corresponding table of EXAFS fitting results is shown in Table S1.

Given the key role of MLC through reversible dearomatization of ligand backbones in catalytic transformations with mononuclear (PNP)Ru complexes, – a feature also possible with  $^t\text{BuPNNP}$  – we investigated the reactivity of complex **1** towards bases. The addition of two equiv of  $\text{KOtBu}^{28}$  to an orange suspension of complex **1** in a mixture of THF/toluene/benzene results in rapid formation of a dark red suspension from which  $[\text{Ru}_2(^t\text{BuPNNP}^*)\text{H}(\mu\text{-H})(\mu\text{-OtBu})(\text{CO})_2](\mathbf{3})$  can be isolated as a red solid in 77% yield (Scheme 2). In contrast to complex **1**, complex **3** is air-sensitive and highly soluble in both apolar and polar solvents. The ATR-IR spectrum of **3** (Fig S28) shows a strong terminal CO band at  $\nu = 1923 \text{ cm}^{-1}$  and a shoulder at  $\nu = 1890 \text{ cm}^{-1}$ . In comparison to **1** and **2** these bands are at significantly lower energies showing that there is increased  $\pi$ -backdonation to the CO ligands in complex **3**. The  $^{31}\text{P}\{^1\text{H}\}$  NMR spectrum of **3** in  $\text{THF-}d_8$  (Fig S21) features two resonances at  $\delta = 104.1$  and  $91.4 \text{ ppm}$  that both are magnetically coupled to the hydride ligands.<sup>29</sup> Four aromatic resonances assigned to the naphthyridine backbone are observed at  $\delta = 6.97, 6.53, 6.46$  and  $6.38 \text{ ppm}$  in the  $^1\text{H}$  NMR spectrum. The upfield shifts of these resonances and that of one of the P atoms in comparison with **2** is consistent with partial dearomatization of the  $^t\text{BuPNNP}$  ligand.<sup>22</sup> This is further supported by the observation of the three resonances at  $\delta = 4.20, 3.45$  and  $3.30 \text{ ppm}$  corresponding to the methine  $\text{CH}$  and diastereotopic methylene  $\text{CH}_2$  protons, respectively. The presence of a tert-butoxide ligand is confirmed by the observation of a singlet at  $\delta = 1.13 \text{ ppm}$  that integrates for nine protons. Furthermore, complex **3** displays two hydride signals ( $\delta = -15.76 \text{ ppm}$ , doublet, and  $-20.97 \text{ ppm}$ , doublet of doublets) with the same coupling patterns as observed for complex **2**, implying that both a terminal and bridging hydride ligand are present. Extensive 2D NMR analysis is also consistent the structure depicted in Scheme 3 featuring a 16 VE Ru center in the dearomatized PN pocket and an 18 VE Ru center featuring a terminal hydride in the neutral PN binding pocket (see ESI for detailed analysis and discussion). Despite numerous attempts, a satisfactory combustion analysis or single-crystals of complex **3** suitable for X-ray diffraction were not obtained.



**Scheme 3:** The synthesis of complex **3** by reaction of **1** with two equiv KOtBu.

A key feature of dearomatized 16 VE count Milstein-type PNL-Ru systems (L = N or P) is their cooperative activation of H<sub>2</sub> to form 18 VE dihydride complexes, which are involved in a variety of catalytic (de)hydrogenative chemical transformations.<sup>16e,30</sup> Hence, we envisioned that the partially dearomatized ligand in complex **3** could enable similar cooperative H<sub>2</sub> activation to mediate the catalytic hydrogenation of unsaturated bonds. To this end, toluene solutions of complex **3** with various unsaturated substrates were exposed to a H<sub>2</sub> atmosphere (1 atmosphere) at ambient temperature for 20 h. Under these conditions, poor conversion was observed for ketones, imines, internal alkenes and terminal alkynes. In contrast, we found that diphenyl acetylene was fully consumed under these mild reaction conditions. GC-MS and NMR analysis of the resulting mixture showed selective conversion to *E*-stilbene, with ~10% of 1,2-diphenylethane. Monitoring the semi-hydrogenation of diphenylacetylene in C<sub>6</sub>D<sub>6</sub> by <sup>1</sup>H NMR spectroscopy using 5 mol% **3** under 1 atm of H<sub>2</sub> atmosphere at 25 °C showed full conversion of diphenylacetylene after 10 h into a mixture of 94% *E*-stilbene and 6% 1,2-diphenylethane (Figure 3). The concentration of *E*-stilbene steadily increases from the start of the experiment, but with a slower rate than the consumption of diphenyl acetylene. This agrees with the observed formation of significant amounts of *Z*-stilbene in the first hours of the reaction. The *Z*-stilbene concentration peaks after approximately 3 hours, after which its concentration decreases slowly over time. Finally, throughout the experiment a steady, yet minor, increase of the concentration of 1,2-diphenylethane is observed. These observations show that complex **3** catalyzes both the semi-hydrogenation of diphenyl acetylene and the *Z*-to-*E* isomerization under mild conditions (see below). Although previous examples of Ru-catalyzed *E*-selective semi-hydrogenation of diphenylacetylene have been reported,<sup>11a,8e</sup> **3** is the most active Ru-based catalysts under these mild conditions.<sup>12,18</sup> As **3** is air and moisture sensitive, we also investigated its *in situ* preparation from air-stable **1** and KOtBu. Gratifyingly, we found similar activity and selectivity using the *in situ* prepared catalyst for the semi-hydrogenation of diphenylacetylene as with isolated **3**.

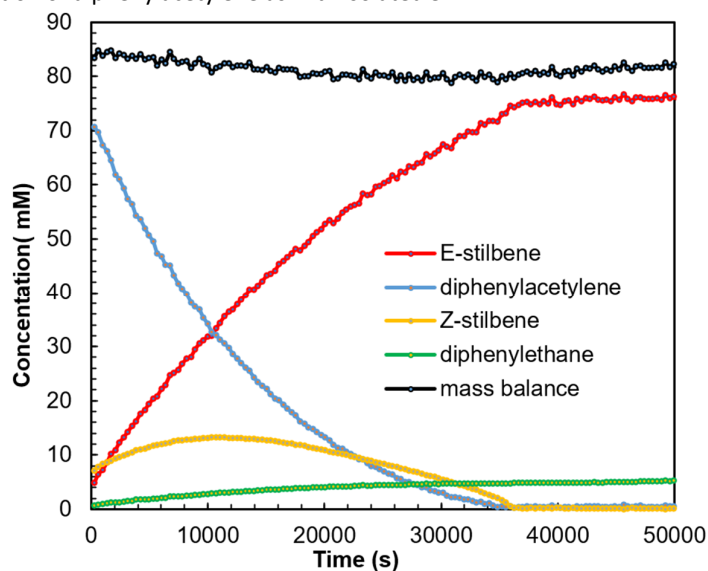
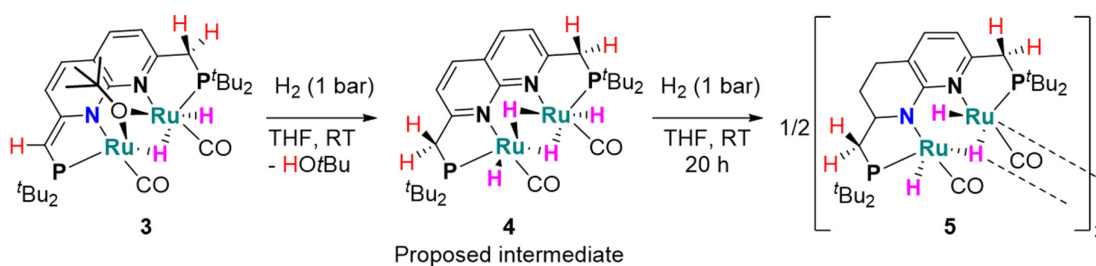


**Figure 3:** Kinetic plot of the hydrogenation of diphenylacetylene catalyzed by complex **3** showing the concentration of the various compounds based on integration of <sup>1</sup>H NMR resonances versus time.

We observed that under the semi-hydrogenation conditions in  $C_6D_6$  the color of the reaction mixture gradually changed from red to brown overnight. Accordingly,  $^{31}P\{^1H\}$  and  $^1H$  NMR spectra of the resulting mixture showed the consumption of complex **3**. To gain insight into this process, more concentrated  $C_6D_6$  and THF- $H_8$  solutions of **3** were subjected to a  $H_2$  atmosphere (1 atm) and analyzed by NMR spectroscopy. In the absence of substrate a similar color change was observed in  $C_6D_6$  after 24 hours concomitant with the formation of an intractable mixture of species based on the  $^{31}P$  and  $^1H$  NMR spectra. In contrast, in THF solution the color of the solution changes from red to red-brown within 30 minutes, concomitant with full conversion of complex **3** to a new species (**4**), which displays a single resonance at  $\delta = 100.2$  ppm in the  $^{31}P$  NMR spectrum in THF- $h_8$  at 298 K (Figure S30). The  $^1H$  NMR spectrum features two doublets at  $\delta = 8.30$  ( $J_{H,H} = 8.2$  Hz) and 7.77 ppm ( $J_{H,H} = 8.2$  Hz) and two different resonances assigned to the methylene linker protons at  $\delta = 3.94$  and 3.18 ppm, and all integrate equally. In addition, two doublets at  $\delta = 1.48$  and 1.18 ppm are assigned to the *t*-Bu substituents. These spectroscopic features are characteristic signs of a  $C_2$ -symmetric species containing an aromatic PNNP backbone.<sup>22c</sup> Additionally, two hydride resonances are observed at  $\delta = -8.85$  (doublet) and  $-12.72$  ppm (doublet of doublets), that together integrate for 4H, showing that four hydride ligands are present. These observations imply the formation of a diruthenium tetrahydride complex as depicted in Scheme 4. Its formation is proposed to involve metal-ligand cooperative  $H_2$  activation and hydrogenolysis of the *tert*-butoxide ligand, which is in agreement with the observed formation of  $HOtBu$  in the  $^1H$  NMR spectrum. Further characterization of complex **4** was hampered due to its instability under  $H_2$  or  $N_2$  atmosphere (see ESI for details).



**Scheme 4:** The cooperative  $H_2$  activation of complex **3** resulting in intermediate **4**, which subsequently is converted to complex **5**.

Notably, longer reaction times (24-48 hours) in either  $C_6D_6$ , toluene or THF results in yellow-brown solutions concomitant with the formation of a new non-symmetric major species  $[(Ru_2(t^BuPNNP^*)H_2(\mu-H)(CO)_2)_2]$  (**5**), which was isolated as a dark brown powder in 41% yield (Scheme 4). The ATR-IR spectrum of **5** displays three terminal carbonyl bands at  $\nu = 1950, 1925$  and  $1897$   $cm^{-1}$ . The  $^{31}P\{^1H\}$  NMR spectrum of complex **5** in  $DCM-d_2$  at 298 K displays two resonances at  $\delta = 106.7$  and 105.0 ppm. In the  $^1H$  NMR spectrum, only two aromatic resonances are observed for complex **5** at  $\delta = 6.33$  and 5.84 ppm together with six resonances with complex coupling patterns. In addition, three resonances are observed at  $\delta = -13.40$  (doublet of doublets),  $-20.25$  (multiplet) and  $-20.46$  ppm (doublet of doublets), showing that **5** contains three hydride signals of which two display mutual coupling (see ESI). Together these findings indicate that the two ruthenium centers have distinct geometries.

Single crystals of complex **5** suitable for X-ray diffraction were grown by layering a concentrated THF solution of **5** with hexane. The solid-state structure (Figure 4) revealed a dimeric species which is located on a twofold rotation axis, comprised out of two  $(PNNP)Ru_2(CO)_2H_3$  fragments that are proposed to share two hydride ligands. The hydride ligands are only weakly supported by the X-ray intensities. Furthermore, as indicated by NMR analysis, **5** contains a partially hydrogenated ligand backbone to form a 1,2,3,4-tetrahydro-1,8-naphthyridine-like ligand backbone (see Scheme 4). The hydrogenation of *N*-heterocyclic backbones in mononucleating pincer ligands has been observed previously, but typically requires high temperatures and  $H_2$  pressures.<sup>31</sup> In contrast, the observed partial backbone hydrogenation in **5** occurs at room temperature and atmospheric pressure. We reason that facile hydrogenation is inherent to the combination of a naphthyridine-

based ligand combined with a diruthenium core given a previous report wherein similar reactivity was observed for a 2,7-bis(2-pyridinyl)-1,8-naphthyridine ligand with  $\text{Ru}_3(\text{CO})_{12}$ .<sup>32</sup> Although both Ru-Ru distances of 2.7364(3) Å (Ru1-Ru2) and 2.8627(4) Å (Ru1-Ru1<sup>i</sup> between the different monomers) are shorter than the sum of the covalent radii, a formal Ru-Ru bond is not expected, just as for complex **2**. Aided by the solid-state structure, extensive 2D NMR analysis enabled assignment of the resonances in the NMR spectra and suggests that the dimeric nature of **5** is retained in solution (see ESI). This is likely due to delocalized 4c2e bond of the hydrides to give 18 VE configuration for all Ru centers in the dimer.

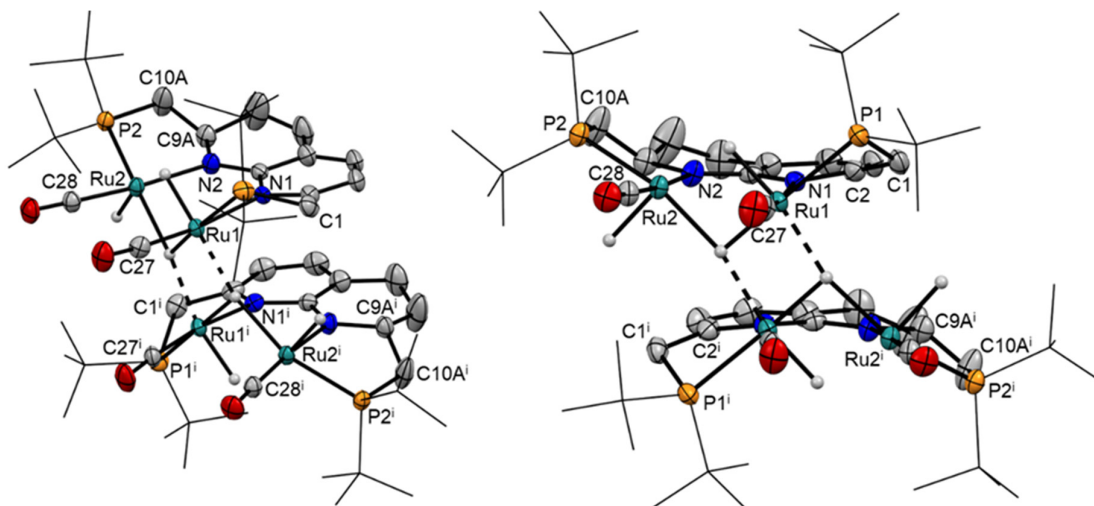


**Figure 4:** Displacement ellipsoid plots (50% probability) of the major disorder component of the molecular structure of **5** in the crystal with the *-t*Bu groups on P depicted as wireframe for clarity (symmetry code *i*: 1-*x*, 1-*y*, *z*). Most hydrogen atoms are omitted, the hydride ligands are tentative. Ru1-Ru2 2.7364(3) Å, Ru1-Ru1<sup>i</sup> 2.8627(4) Å, Ru1-P1 2.3016(8) Å, Ru1-N1 2.165(3) Å, Ru1-C27 1.828(4) Å, Ru2-P2 2.2466(8) Å, Ru2-N2 2.149(3) Å, Ru2-C28 1.833(3) Å, C1-C2 1.500(5) Å, C9A-C10A 1.414(9) Å.

With these insights into the fate of the complex **3** under the semi-hydrogenation conditions, we reanalyzed the NMR spectra from the hydrogenation experiments of diphenylacetylene and found that complex **5** is progressively formed during the hydrogenation experiments. Hence, we investigated the activity and selectivity of complex **5** as a catalyst for the hydrogenation of diphenylacetylene under identical conditions (Figure 5). Interestingly, the kinetic profile of complex **5** is markedly different compared to that of complex **3**. A significantly slower conversion of diphenylacetylene is observed as after 14 h, only 31% of the diphenylacetylene is converted and all three expected hydrogenation products, *Z*-stilbene, *E*-stilbene and 1,2-diphenylethane are observed. Although the *E*-stilbene is the major product (17%) after 14 h, 7% *Z*-stilbene and 6% of 1,2-diphenylethane are also formed. This shows that **5** is a significantly less active and selective catalyst than complex **3** under these conditions.

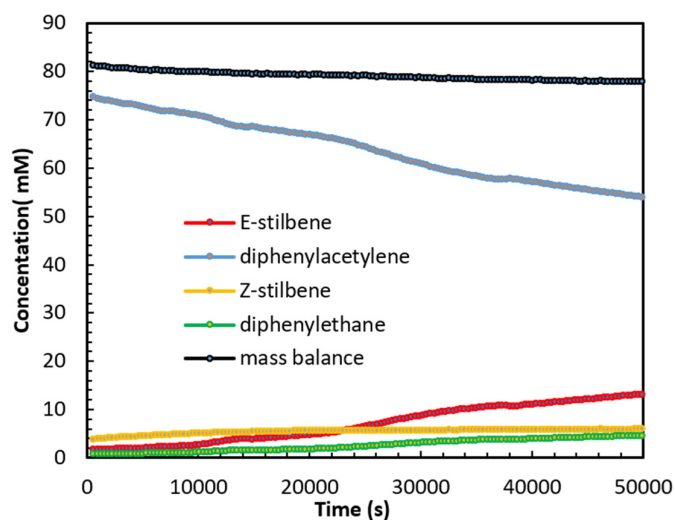


**Figure 5:** Kinetic plot of the hydrogenation of diphenylacetylene catalyzed by complex **5** showing the concentration of the various compounds based on integration of  $^1\text{H}$  NMR resonances versus time.

For comparison we also investigated the catalytic activity and product selectivity of Milstein's monometallic 16 VE count  $[\text{Ru}(\text{t}^{\text{Bu}}\text{PNP}^*)\text{H}(\text{CO})]$  complex<sup>17c</sup> as a catalyst for the semi-hydrogenation of diphenylacetylene under identical conditions (Figure S62). Notably, the rate of diphenylacetylene conversion is lower than that observed for both complexes **3** and **5** and 1,2-diphenylethane is the major product throughout the course of the reaction, and only minor amounts of *E*-stilbene and *Z*-stilbene are observed.

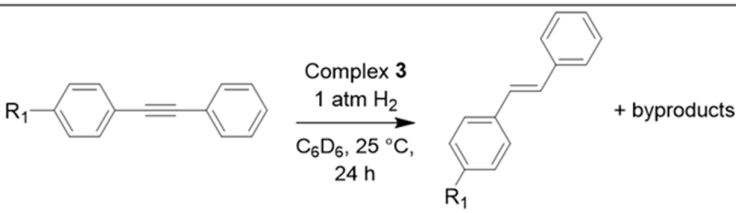
The kinetic profile in Figure 3 suggests that initially diphenylacetylene is hydrogenated to give a mixture of both stilbenes, but that *Z*-stilbene is isomerized to *E*-stilbene. A control experiment wherein *Z*-stilbene was added to a  $\text{C}_6\text{D}_6$  solution containing complex **3** (5 mol%) showed full conversion to *E*-stilbene within 10 minutes. This shows that the isomerization of *Z*-stilbene already occurs with exclusion of a  $\text{H}_2$  atmosphere. Subsequent exposure of this mixture to a  $\text{H}_2$  atmosphere (1 bar), showed only minor conversion ( $\sim 5\%$ ) to 1,2-diphenylethane and conversion of **3** to **5** after 16 h. These results indicate that complex **3** is a potent catalyst for the *Z*-to-*E* isomerization of *Z*-stilbene. Although complex **5** is not as active as complex **3** in the semi-hydrogenation of diphenylacetylene, its catalytic activity for the isomerization of *Z*-stilbene to *E*-stilbene is comparable to that of **3** as full conversion is also observed within 10 min (using 5 mol% **5**, see ESI for details). The observation that *Z*-stilbene is present throughout the course of the semi-hydrogenation of diphenylacetylene (Figure 3) shows that something inhibits the alkene isomerization by **3** or **5**. We found that the fast isomerization of *Z*-stilbene to *E*-stilbene catalyzed by **3** or **5** was unaffected by placing the reaction mixture under a  $\text{H}_2$  atmosphere. In contrast, when **3** or **5** (5 mol%) was added to an equimolar mixture of diphenylacetylene no isomerization of *Z*-stilbene occurs. This illustrates that the alkyne substrate inhibits the isomerization of *Z*-alkenes and explains the increased rate of consumption of *Z*-stilbene in Figure 3 when diphenylacetylene is nearly consumed.

Given our findings that **3** is a poor hydrogenation catalyst for ketones, imines, internal alkenes and terminal alkynes under the explored reaction conditions (see above), we set out to investigate the functional group tolerance of the *E*-selective semi-hydrogenation of alkynes catalyzed by **3**. Towards this end we exposed a series of substituted alkynes to a  $\text{H}_2$  atmosphere (1 atm) at 25 °C in the presence of 5 mol% **3** for 24 hours (Table 1). These substrates contain fragments that are prone to be reduced in metal-catalyzed hydrogenation reactions. Note that these conditions are not optimized for a particular substrate but were chosen to enable comparison of how the various functional groups affect the conversion, selectivity, and mass balance of the reactions.

Diphenylacetylene (entry 1) was fully consumed after 24 h under these conditions to the *E*-alkene and 11% of the alkane product. This is in line with our findings described above, albeit with more alkane formation

due to the longer reaction time. Similar conversion and selectivity is observed when an electron withdrawing methyl ester is placed on the para position of one of the phenyl groups (entry 2). In contrast, only 45% conversion was observed for the substrate with nitrile group in this position (entry 3). With this substrate we also found predominant formation of the Z-alkene, similar to what was observed recently by Turculet and coworkers.<sup>13</sup> However, we found that performing the same reaction at 40 °C (entry 4) results in full conversion of the substrate and 91% selectivity for the E-alkene. The aldehyde bearing substrate showed slightly higher conversion under the standard conditions, but also predominantly gave the Z-alkene (entry 5). Longer reaction times (entry 6) did result in full conversion, but no significant change in E/Z selectivity. Performing the same reaction at 40 °C (entry 7) resulted in full isomerization to the E-alkene, but also resulted in significant formation of the alkene product wherein the aldehyde was reduced to the alcohol. This product also partially precipitated resulting in a lower observed mass balance. Interestingly, the substrate substituted with an imine group (entry 8) showed full conversion under the standard conditions with decent selectivity towards the E-alkene. The main side product in this reaction was the alkene product wherein the imine was hydrogenated to the amine, which also partially precipitated from the reaction mixture. The substrate containing an electron donating methoxy group (entry 9) was also found to react slower than the parent diphenylacetylene, but was fully converted after longer reaction times with comparable selectivity (entry 10). Overall, relatively minor formation of the alkane product is observed (~5-10%) for all substrates, and good functional group tolerance is observed.

**Table 1:** Hydrogenation of diphenylacetylenes using complex 3.



Entry	R <sub>1</sub>	Conversion	Z-alkene	E-alkene	alkane	byproducts	Mass balance
1	H	100%	0%	88%	11%	0%	99%
2	COOMe	100%	0%	85%	11%	0%	96%
3	CN	45%	32%	0%	3%	0%	90%
4 <sup>a</sup>	CN	100%	0%	91%	6%	0%	97%
5	HC=O	85%	52%	27%	2%	3% (alcohol product)	99%
6 <sup>b</sup>	HC=O	99%	52%	31%	2%	5% (alcohol product)	89%
7 <sup>a</sup>	HC=O	100%	0%	29%	1%	53% (E-alkene alcohol)	83% <sup>c</sup>
8	HC=N-Ph	100%	0%	65%	6%	11% (amine)	82% <sup>c</sup>
9	OMe	86%	8%	67%	8%	0%	97%
10 <sup>b</sup>	OMe	100%	0%	83%	9%	0%	92%

Reaction conditions: Substrate (50 μmol), complex 3 (5 mol%) were dissolved in 0.60 mL C<sub>6</sub>D<sub>6</sub> at 25 °C under 1 atm of H<sub>2</sub> for the time described. Spectroscopic yields were determined with mesitylene (3 μL) as internal standard using <sup>1</sup>H NMR spectroscopy. <sup>a</sup> Reaction at 40 °C. <sup>b</sup> Reaction for 48 h. <sup>c</sup> The poor mass balance is due to product precipitation.

Interestingly, for most substrates the metal complex observed in solution prior to and after H<sub>2</sub> addition is complex 3, indicating that an alkyne insertion product into a Ru-H bond is not the catalyst resting state. However, for both the aldehyde and nitrile substituted substrates we observed a color change upon mixing with the catalyst that was not observed for the other substrates. Moreover, no complex 3 was observed in the <sup>1</sup>H NMR spectra of these mixtures. We propose that competition between the coordination of these functional groups and the alkyne moiety to ruthenium(II), results in a slower reaction. Future research will focus on

expanding the substrate scope, reaction optimization and obtaining detailed insights into the mechanism of alkyne semi-hydrogenation by these diruthenium(II) hydride complexes.

## Conclusion

In conclusion, the <sup>t</sup>BuPNNP ligand grants access to a new class of diruthenium(II) hydrido carbonyl complexes. These complexes show semblance to Milstein's monometallic PNP ruthenium(II) hydrido carbonyl complexes and display similar metal-ligand cooperative activation of H<sub>2</sub>. However, unlike their mononuclear counterparts they are active catalysts for the *E*-selective semi-hydrogenation of diphenyl acetylenes. To the best of our knowledge, the reported diruthenium system is the most active Ru-based system for this transformation, which can be performed at room temperature and 1 atm of H<sub>2</sub>. Moreover, a variety of functional groups that are sensitive to hydrogenation are tolerated with only aldehydes and imines showing partial conversion to the respective alcohol and amine. Preliminary mechanistic investigations suggest a mechanism that involves hydrogenation to the *Z*-alkene followed by catalytic *Z*-to-*E* isomerization, which is inhibited by the alkyne substrate. Moreover, a key polyhydride species was spectroscopically observed and a deactivated species was characterized, which features a partially hydrogenated ligand backbone.

In addition to further optimization of the reaction conditions and functional group tolerance, future research in our group will focus on obtaining insights into the mechanism of the *E*-selective semi-hydrogenation of alkynes catalyzed by the described diruthenium complexes. We will particularly focus on the role of cooperative interplay of the two ruthenium centers in this and other (de)hydrogenative transformations.

## Supporting information

Experimental procedures and details, NMR spectra, and computational and crystallographic computational details can be found in the ESI. In addition, NMR and computational data files can be obtained from the 4TU database under DOI: xxxxx. CCDC 2160732-2160733 contain the supplementary crystallographic data for this paper.

## Conflicts of interest

There are no conflicts to declare.

## Acknowledgements

This work was supported by The Netherlands Organization for Scientific Research (START-UP grant 740.018.019 to D. L. J. B.). Access to supercomputer facilities was sponsored by NWO Exacte en Natuurwetenschappen (Physical Sciences). Marc-Etienne Moret is acknowledged for valuable discussions and suggestions. The X-ray diffractometer was financed by the NWO.

Stanford Synchrotron Radiation Lightsource, SLAC National Accelerator Laboratory, is supported by the U.S. Department of Energy, Office of Science, Office of Basic Energy Sciences. RS and ASA are supported by the U.S. Department of Energy, Office of Energy Efficiency and Renewable Energy (EERE), Advanced Manufacturing Office (AMO) and Bioenergy Technologies Office (BETO) as part of the BOTTLE™ Consortium, funded under contract no. DE-AC36-08GO28308 with the National Renewable Energy Laboratory.

## References

- 
- <sup>1</sup> (a) Thomas, S. P.; Greenhalgh, M.D., Heterogeneous Hydrogenation of C=C and C C bonds in *Comprehensive Organic Synthesis*: Elsevier, 2014, Vol. 8, p 564. (b) Ager, D., Homogeneous Catalytic Hydrogenation of C=C and C C bonds in *Comprehensive Organic Synthesis*: Elsevier, 2014, Vol. 8, p 605. (c) Crespo-Quesada, M.; Cárdenas-

Lizana, F.; Dessimoz, A.-L.; Kiwi-Minsker, L., Modern Trends in Catalyst and Process Design for Alkyne Hydrogenations. *ACS Catal.* **2012**, *2*, 1773–1786. (d) Chinchilla, R.; Nájera, C., Chemicals from Alkynes with Palladium Catalysts. *Chem. Rev.* **2014**, *114*, 1783–1826. (e) Molnár, Á.; Sárkány, A.; Varga, M., Hydrogenation of carbon–carbon multiple bonds: chemo-, regio- and stereo-selectivity. *J. Mol. Catal. A: Chem.* **2001**, *173*, 185–221.

<sup>2</sup> (a) Lindlar, H.; Dubuis, R, Palladium Catalyst for Partial Reduction of Acetylenes in *Organic Syntheses*; Wiley, 1966; Vol. 46, p 89. (b) H.-U. Blaser, A. Schnyder, H. Steiner, F. Rössler, P. Baumeister in Handbook of Heterogeneous Catalysis, Vol. 7, 2nd ed. (Eds.: G. Ertl, H. Knözinger, F. Schüth, J. Weitkamp), Wiley-VCH, Weinheim, 2008, pp. 3284–3308

<sup>3</sup> A. M. Kluwer, C. J. Elsevier in Handbook of Homogeneous Hydrogenation, Vol. 1 (Eds.: J. G. de Vries, C. J. Elsevier), Wiley-VCH, Weinheim, 2007, pp. 375–411f

<sup>4</sup> (a) Schrock, R. R.; Osborn, J. A. Catalytic Hydrogenation Using Cationic Rhodium Complexes. II. The Selective Hydrogenation of Alkynes to Cis Olefins. *J. Am. Chem. Soc.* **1976**, *98*, 2143–2147. (b) Crabtree, R. H.; Gautier, A.; Giordano, G.; Khan, T. The preparation and some catalytic properties of a number of rhodium(I) diolefin complexes. *J. Organomet. Chem.* **1977**, *141*, 113–121.

<sup>5</sup> Pasto, D. J. Reductions of CC and CC by Noncatalytic Chemical Methods. In Comprehensive Organic Synthesis; Trost, B. M., Fleming, I., Eds.; Pergamon Press: Oxford, U.K., 1991, Vol.8, p 471–488.

<sup>6</sup> Add here recent examples showing *E*-selective semi-hydrogenation of alkynes

<sup>7</sup> (a) Radkowski, K.; Sundararaju, B.; Fürstner, A. A Functional-Group-Tolerant Catalytic trans Hydrogenation of Alkynes. *Angew. Chem., Int. Ed.* **2013**, *52*, 355–360. (b) Leutzsch, M.; Wolf, L. M.; Gupta, P.; Fuchs, M.; Thiel, W.; Farès, C.; Fürstner, A. Formation of Ruthenium Carbenes by gem-Hydrogen Transfer to Internal Alkynes: Implications for Alkyne trans-Hydrogenation. *Angew. Chem., Int. Ed.* **2015**, *54*, 12431–12436. (c) Guthertz, A.; Leutzsch, M.; Wolf, L. M.; Gupta, P.; Rummelt, S. M.; Goddard, R.; Farès, C.; Thiel, W.; Fürstner, A. Half-Sandwich Ruthenium Carbene Complexes Link trans-Hydrogenation and gem-Hydrogenation of Internal Alkynes. *J. Am. Chem. Soc.* **2018**, *140*, 3156–3169. (d) Biberger, T.; Gordon, C. P.; Leutzsch, M.; Peil, S.; Guthertz, A.; Copéret, C.; Fürstner, A. Alkyne gem-Hydrogenation: Formation of Pianostool Ruthenium Carbene Complexes and Analysis of Their Chemical Character. *Angew. Chem., Int. Ed.* **2019**, *58*, 8845–8850.

<sup>8</sup> (a) Srimani, D.; Diskin-Posner, Y.; Ben-David, Y.; Milstein, D. Iron Pincer Complex Catalyzed, Environmentally Benign, *E*-Selective Semi-Hydrogenation of Alkynes. *Angew. Chem., Int. Ed.* **2013**, *52*, 14131–14134. (b) Tokmic, K.; Fout, A. R. Alkyne Semihydrogenation with a Well-Defined Nonclassical Co–H<sub>2</sub> Catalyst: A H<sub>2</sub> Spin on Isomerization and *E*-Selectivity. *J. Am. Chem. Soc.* **2016**, *138*, 13700–13705. (c) Gramigna, K. M.; Dickie, D. A.; Foxman, B. M.; Thomas, C. M. Cooperative H<sub>2</sub> Activation across a Metal–Metal Multiple Bond and Hydrogenation Reactions Catalyzed by a Zr/Co Heterobimetallic Complex. *ACS Catal.* **2019**, *9*, 3153–3164. (d) Murugesan, K.; Bheeter, C. B.; Linnebank, P. R.; Spannenberg, A.; Reek, J. N. H.; Jagadeesh, R. V.; Beller, M. Nickel-Catalyzed Stereodivergent Synthesis of *E*- and *Z*-Alkenes by Hydrogenation of Alkynes. *ChemSusChem* **2019**, *12*, 3363–3369. (e) Karunananda, M. K.; Mankad, N. P. *E*-Selective Semi-Hydrogenation of Alkynes by Heterobimetallic Catalysis. *J. Am. Chem. Soc.* **2015**, *137*, 14598–14601. (f) Karunananda, M. K.; Mankad, N. P. Heterobimetallic H<sub>2</sub> Addition and Alkene/Alkane Elimination Reactions Related to the Mechanism of *E*-Selective Alkyne Semihydrogenation. *Organometallics* **2017**, *36*, 220–227. (g) Muhammad, S. R.; Nugent, J. W.; Tokmic, K.; Zhu, L.; Mahmoud, J.; Fout, A. R. Electronic Ligand Modifications on Cobalt Complexes and Their Application toward the Semi-Hydrogenation of Alkynes and Para-Hydrogenation of Alkenes. *Organometallics* **2019**, *38*, 3132–3138. (h) Higashida, K.; Mashima, K., *Chem. Lett.* **2016**, *45*, 866–868.

<sup>9</sup> Maazaoui, R.; Abderrahim, R.; Chemla, F.; Ferreira, F.; Perez-Luna, A.; Jackowski, O. Catalytic Chemoselective and Stereoselective Semihydrogenation of Alkynes to *E*-Alkenes Using the Combination of Pd Catalyst and ZnI<sub>2</sub>. *Org. Lett.* **2018**, *20*, 23, 7544–7549.

<sup>10</sup> In transfer hydrogenation: Wang, Y.; Huang, Z.; Huang, Z. Catalyst as colour indicator for endpoint detection to enable selective alkyne trans-hydrogenation with ethanol. *Nat. Cat.* **2019**, Vol. 2, 529–536.

<sup>11</sup> (a) Tseng, K.-N. T.; Kampf, J. W.; Szymczak, N. K. Modular Attachment of Appended Boron Lewis Acids to a Ruthenium Pincer Catalyst: Metal–Ligand Cooperativity Enables Selective Alkyne Hydrogenation. *J. Am. Chem. Soc.* **2016**, *138*, 10378–10381. (b) using alcohol as H<sub>2</sub> source: Ekebergh, A.; Begon, R.; Kann, N. Ruthenium-Catalyzed *E*-Selective Alkyne Semihydrogenation with Alcohols as Hydrogen Donors. *J. Org. Chem.* **2020**, *85*, 2966–2975.

- <sup>12</sup> Takemoto, S.; Kitamura, M.; Saruwatari, S.; Isono, A.; Takda, Y.; Nishimori, R.; Tsujiwaki, M.; Sakaue, N.; Matsuzaka, H. Bis(bipyridine) ruthenium(ii) bis(phosphido) metalloligand: synthesis of heterometallic complexes and application to catalytic (*E*)-selective alkyne semi-hydrogenation. *Dalton Trans.*, **2019**, *48*, 1161-1165.
- <sup>13</sup> Hale, D. J.; Ferguson, M. J.; Turculet, L. (PSiP)Ni-Catalyzed (*E*)-Selective Semihydrogenation of Alkynes with Molecular Hydrogen. *ACS Catal.* **2022**, *12*, 2253–2260.
- <sup>14</sup> Ramirez, B. L.; Lu, C. C. Rare-Earth Supported Nickel Catalysts for Alkyne Semihydrogenation: Chemo- and Regioselectivity Impacted by the Lewis Acidity and Size of the Support. *J. Am. Chem. Soc.* **2020**, *142*, 5396–5407; (
- <sup>15</sup> (a) Michaelides, I. N.; Dixon, D. J. Catalytic Stereoselective Semihydrogenation of Alkynes to *E*-Alkenes. *Angew. Chem. Int. Ed.* **2013**, *52*, 806-808. (b) Thiel, N. O.; Kaewmee, B.; Ngoc, T. T.; Teichert, J. F. A Simple Nickel Catalyst Enabling an *E*-Selective Alkyne Semihydrogenation. *Chem. Eur. J.* **2020**, *26*, 1597-1603.
- <sup>16</sup> (a) Van Koten, G.; Kirchner, K.; Moret, M.-E. Metal–Ligand Co-operativity, Topics in Organometallic Chemistry, 2021, vol. 68. (b) Elsby, M. R.; Baker, R. T. Strategies and mechanisms of metal–ligand cooperativity in first-row transition metal complex catalysts. *Chem. Soc. Rev.*, **2020**, *49*, 8933–8987. (c) Higashi, T.; Kusumoto, S.; Nozaki, K. Cleavage of Si–H, B–H, and C–H Bonds by Metal–Ligand Cooperation. *Chem. Rev.*, **2019**, *119*, 10393–10402. (d) Alig, L.; Fritz, M.; Schneider, S. First-Row Transition Metal (De)Hydrogenation Catalysis Based On Functional Pincer Ligands. *Chem. Rev.*, **2019**, *119*, 2681–2751. (e) Khusnutdinova, J. R.; Milstein, D. Metal–Ligand Cooperation. *Angew. Chem., Int. Ed.*, **2015**, *54*, 12236–12273.
- <sup>17</sup> (a) Gunanathan, C.; Ben-David, Y.; Milstein, D. Direct Synthesis of Amides from Alcohols and Amines with Liberation of H<sub>2</sub>. *Science* **2007**, *317* (5839), 790–792. (b) Zhang, J.; Gandelman, M.; Shimon, L. J. W.; Rozenberg, H.; Milstein, D. Electron-Rich, Bulky Ruthenium PNP-Type Complexes. Acceptorless Catalytic Alcohol Dehydrogenation. *Organometallics* **2004**, *23* (17), 4026–4033. (c) Gnanaprakasam, B.; Zhang, J.; Milstein, D. Direct Synthesis of Imines from Alcohols and Amines with Liberation of H<sub>2</sub>. *Angew. Chem. Int. Ed.* **2010**, *49* (8), 1468–1471.
- <sup>18</sup> At the time of editing this manuscript a pre-print by Milstein and co-workers was posted on ChemRxiv detailing an acridine-based PNP platform for the semi-hydrogenation of alkynes: *ChemRxiv*, DOI: [10.26434/chemrxiv-2022-3wt11](https://doi.org/10.26434/chemrxiv-2022-3wt11)
- <sup>19</sup> (a) Iglesias, M.; Sola, E.; Oro, L. A. in Homo- and Heterobimetallic Complexes in Catalysis: Cooperative Catalysis, ed. P. Kalck, Springer International Publishing, Cham, **2016**, pp. 31–58. (b) Mankad, N. P. Selectivity Effects in Bimetallic Catalysis. *Chem. Eur. J.* **2016**, *22*, 5822–5829; (c) Pye, D. R.; Mankad, N. P. Bimetallic catalysis for C–C and C–X coupling reactions. *Chem. Sci.* **2017**, *8*, 1705–1718. (d) Farley, C. M.; Uyeda, C. Organic Reactions Enabled by Catalytically Active Metal–Metal Bonds. *Trends Chem.* **2019**, *1*, 497–509. (e) Xiong, N.; Zhang, G.; Sun, X.; Zeng, R. Metal-Metal Cooperation in Dinucleating Complexes Involving Late Transition Metals Directed towards Organic Catalysis. *Chin. J. Chem.*, **2020**, *38*, 185–201. (f) Rey, S.; Tsurugi, H.; Mashima, K. *Coord. Chem. Rev.* **2018**, *355*, 223–239. (g) Maity, R.; Birenheide, B. S.; Breher, F.; Sarkar, B. *ChemCatChem* **2021**, *13*, 2337–2370.
- <sup>20</sup> Desnoyer, A. N.; Nicolay, A.; Rios, P.; Ziegler, M. S.; Tilley, T. D. Bimetallics in a Nutshell: Complexes Supported by Chelating Naphthyridine-Based Ligands. *Acc. Chem. Res.* **2020**, *53*, 1944–1956. (a) He, C.; Barrios, A. M.; Lee, D.; Kuzelka, J.; Davydov, R. M.; Lippard, S. J. Diiron Complexes of 1,8-Naphthyridine-Based Dinucleating Ligands as Models for Hemerythrin. *J. Am. Chem. Soc.*, **2000**, *122*, 12683–12690. (b) He, C.; Dubois, J. L.; Hedman, B.; Hodgson, K. O.; Lippard, S. J. A Short Copper-Copper Distance in a (μ-1,2-Peroxy)dicopper(II) Complex Having a 1,8-Naphthyridine Unit as an Additional Bridge. *Angew. Chem. Int. Ed.*, **2001**, *40*, 1484–1487. (c) Bera, J. K.; Sadhukhan, N.; Majumdar, M. 1,8-Naphthyridine Revisited: Applications in Dimetal Chemistry. *Eur. J. Inorg. Chem.* **2009**, *27*, 4023–4038; (d) Sarkar, M.; Doucet, H.; Bera, J. K. Room temperature C–H bond activation on a [Pd–Pd'] platform. *Chem. Commun.* **2013**, *49*, 9764–9766.
- <sup>21</sup> (a) Desnoyer, A. N.; Nicolay, A.; Rios, P.; Ziegler, M. S.; Tilley, T. D. Bimetallics in a Nutshell: Complexes Supported by Chelating Naphthyridine-Based Ligands. *Acc. Chem. Res.* **2020**, *53*, 1944–1956. (b) Wang, Q.; Brooks, S. H.; Liu, T.; Tomson, N. C. Tuning metal–metal interactions for cooperative small molecule activation. *Chem. Commun.* **2021**, *57*, 2839-2853.
- <sup>22</sup> (a) Kounalis, E.; Lutz, M.; Broere, D. L. J. Cooperative H<sub>2</sub> Activation on Dicopper(I) Facilitated by Reversible Dearomatization of an “Expanded PNNP Pincer” Ligand. *Chem. Eur. J.* **2019**, *25* (58), 13280-13284. (b) Kounalis, E.; Lutz, M.; Broere, D. L. J. Tuning the Bonding of a μ-Mesityl Ligand on Dicopper(I) through a Proton-Responsive Expanded PNNP Pincer Ligand. *Organometallics* **2020**, *39* (4), 585-592; (c) van Beek, C.B.; van Leest, N. P.; Lutz, M.; Klein Gebbink, R.J.M.; de Bruin, B.; Broere, D.L.J. Combining Metal-Metal Cooperativity, Metal-Ligand

- 
- Cooperativity and Chemical Non-Innocence in Diiron Carbonyl Complexes *Chem. Sci.*, **2022**, *13*, 2094-2104. (d) Bienenmann, R.L.M; Schanz, A. J.; Ooms, P.L.; Lutz, M.; Broere, D.L.J. A Well-Defined Anionic Dicopper(I) Monohydride Complex that Reacts like a Cluster *Angewandte Chem.* **2022** DOI: 10.1002/anie.202202318
- <sup>23</sup> A yield up to 73% can be achieved, with small loss of purity (see ESI).
- <sup>24</sup> (a) Green, J. C.; Green, M. L. H.; Parkin, G. The Occurrence and Representation of Three-Centre Two-Electron Bonds in Covalent Inorganic Compounds. *Chem. Commun.* **2012**, *48* (94), 11481–11503. (b) Parkin, G. Metal–Metal Bonding in Bridging Hydride and Alkyl Compounds. In *Metal–Metal Bonding*, 2010.
- <sup>25</sup> Cherepakhin, V.; Williams, T. J. Catalyst Evolution in Ruthenium-Catalyzed Coupling of Amines and Alcohols. *ACS Catal.* **2020**, *10* (1), 56–65.
- <sup>26</sup> This is based on the distorted octahedral coordination environment and 18 valence electron count, which suggest no formal Ru–Ru bonding. Additionally, other diruthenium(II) compounds in the work of Bera et al. (*Organometallics* **2016**, *35* (10), 1505–1513) and Petrukhina et al. (*Inorg. Chem.* **2006**, *45* (2), 744–751) show Ru(II) – Ru(II) double bonds around 2.3 Å in length, notably shorter than 2.8 Å.
- <sup>27</sup> (a) Polenova, T.; Gupta, R.; Goldbourt, A. Magic Angle Spinning NMR Spectroscopy: A Versatile Technique for Structural and Dynamic Analysis of Solid-Phase Systems. *Anal. Chem.* **2015**, *87* (11), 5458–5469. (b) Harris, R. K. NMR Studies of Organic Polymorphs & Solvates. *Analyst* **2006**, *131* (3), 351–373.
- <sup>28</sup> Similar experiments using one equiv of KOtBu lead to complex **3** as well, albeit in lower yields.
- <sup>29</sup> The coupling patterns in the otherwise proton decoupled <sup>31</sup>P NMR spectrum are likely caused by coupling to the hydrides, which, due to their low chemical shift can fall outside of the range of the proton decoupler.
- <sup>30</sup> Gunanathan, C.; Milstein, D. Metal–Ligand Cooperation by Aromatization–Dearomatization: A New Paradigm in Bond Activation and “Green” Catalysis. *Acc. Chem. Res.* **2011**, *44*, 8, 588–602..
- <sup>31</sup> Miura, T.; Held, I. E.; Oishi, S.; Naruto, M.; Saito, S. Catalytic Hydrogenation of Unactivated Amides Enabled by Hydrogenation of Catalyst Precursor. *Tetrahedron Lett.* **2013**, *54*, 2674–2678. (b) Miura, T.; Naruto, M.; Toda, K.; Shimomura, T.; Saito, S. Multifaceted Catalytic Hydrogenation of Amides via Diverse Activation of a Sterically Confined Bipyridine–Ruthenium Framework. *Sci. Rep.* **2017**, *7*, 1586. (c) Dawe, L. N.; Karimzadeh-Younjali, M.; Dai, Z.; Khaskin, E.; Gusev, D. G. The Milstein Bipyridyl Pincer Complex of Ruthenium Becomes a Noyori-Type Catalyst under Reducing Conditions. *J. Am. Chem. Soc.* **2020**, *142*, 46, 19510–19522. (d) Deolka, S.; Fayzullin, R. R.; Khaskin, E. Bulky PNP Ligands Blocking Metal-Ligand Cooperation Allow for Isolation of Ru(0), and Lead to Catalytically Active Ru Complexes in Acceptorless Alcohol Dehydrogenation. *Chem. Eur. J.* **2022**, *28*, 4, e202103778.
- <sup>32</sup> Liao, B.-S.; Liu, Y.-H.; Peng, S.-M.; Rajender Reddy, K.; Liu, S.-H.; Chao, P.-T.; Liu, S.-T. An unexpected semi-hydrogenation of a ligand in the complexation of 2,7-bispyridinyl-1,8-naphthyridine with Ru<sub>3</sub>(CO)<sub>12</sub>. *Dalton Trans.* **2014**, *43*, 3557-3562.